Modern Physics Letters A

IMPLEMENTATION OF THE CMS-TOP-18-003 ANALYSIS IN THE MADANALYSIS 5 FRAMEWORK

LUC DARMÉ[1] and BENJAMIN FUKS[2,3]

[1] *Istituto Nazionale di Fisica Nucleare, Laboratori Nazionali di Frascati, C.P. 13, 00044 Frascati, Italy*

[2] *Sorbonne Université, CNRS, Laboratoire de Physique Théorique et Hautes Énergies, LPTHE, F-75005 Paris, France*

[3] *Institut Universitaire de France, 103 boulevard Saint-Michel, 75005 Paris, France*

We present the implementation in MadAnalysis 5 of the CMS-TOP-18-003 search for the production of four top quarks in the Standard Model, and detail the validation of this implementation. This CMS analysis studies Standard Model four-top production through the same-sign and multi-lepton plus jets channels, using a luminosity of 137 fb^{-1} of proton-proton collisions at a centre-of-mass energy of 13 TeV. We validate our implementation work by studying various distributions and event counts describing the properties of the signal in the context of the Standard Model: jet and b-jet multiplicities, the hadronic activity H_T, and the number of expected events populating the various analysis signal regions. We then provide a small example of usage of this implementation to constrain a toy new physics model.

Keywords: four top quark production; top-philic new physics

1. Introduction

In the Standard Model (SM), four top quark production at the LHC ($pp \to t\bar{t}t\bar{t}$) mainly proceeds through pure QCD contributions and the associated production of a top-antitop pair with a Higgs boson in an s-channel-like topology. The total production cross section is predicted, at the next-to-leading order accuracy in the strong coupling, to be $\sigma_{4t}^{\rm SM} = 11.97^{+2.15}_{-2.51}$ fb [1]. By virtue of the size of the top Yukawa coupling, Higgs-boson exchange diagrams contribute significantly. Four-top probes, which have already been under deep scrutiny until now [2–4], have been consequently expected to provide soon an alternative channel to measure the top Yukawa coupling and more generally to play a key role at the upcoming third run of the LHC.

The four-top channel is in addition expected to be important in the search for new physics scenarios, as such a signature could be representative of a variety of new physics scenarios featuring top-philic new scalar or vector particles [5–9]. Such particles arise for instance in composite Higgs solutions to the hierarchy problem [10–14], in models featuring extended supersymmetry [15–22], in models derived from the minimal flavour violation principle [23, 24], but also simply when the new physics

interact with the SM via a scalar portal mechanism (for which the top Yukawa coupling dominates the interactions). Furthermore, four-top production can often be associated with a significant production of missing energy (although in that case supersymmetry-driven searches are typically better suited [25]. While we will not focus on this mass range in this note, the case of a top-philic particle with mass below m_t has been also considered in the literature [26]. Finally, the measurement of the top Yukawa itself can be used to indirectly probe new physics.

New physics contributions generally lead to an enhancement of four-top production, such an enhancement featuring kinematical properties significantly distinct from the SM. It is therefore crucial to be able to extract reasonable bounds on models under consideration from SM four-top production searches, as well as to study the properties of the corresponding new physics signal to design a better suited analysis strategy fully dedicated to the quest for beyond standard model particles. The MadAnalysis 5 platform [27–30] is one of the public software aiming at such an objective. It allows for the derivation of predictions detailing how the different signal regions of a given LHC analysis are populated by an arbitrary new physics signal. The analysis impact on the signal properties can furthermore be estimated.

We present in this note the implementation of the latest CMS analysis targeting the production of four top quarks in the Standard Model [4] in the MadAnalysis 5 framework, briefly describing the analysis itself in Sec. 2. In Sec. 3, we provide information on the procedure that we have followed in order to validate our implementation, so that any potential user can check how robust is our work and to which level any phenomenological outcome should be trusted. In this context, we have verified the compatibility between a SM four-top signal as obtained with our implementation and the official results as reported by the CMS collaboration, both for event counts in the different signal regions of the analysis and various differential distributions. A practical recasting example is shown in Sec. 4 and a summary of our work is given in Sec. 5.

2. Description of the analysis

The production of four top quarks and their subsequent decay at the LHC typically leads to final states featuring a large number of leptons and hard jets with an important heavy-flavour content. In particular, a pair of leptons carrying the same electric charge typically arises from 10% of the decays. In contrast to any other channel, a same-sign di-lepton probe is known to enjoy a low SM background, and is thus an excellent way to search for any new phenomenon. In order to increase the signal efficiency, the analysis additionally considers a final-state with more than two leptons, as the SM background is in that case is also known to be reducible to a small enough level.

2.1. *Object definitions*

The CMS-TOP-18-003 analysis [4] defines 14 signal regions that differ in the details on the selection criteria on the leptons and jets reconstructed in the events. The signal object candidates are required to satisfy mild kinematics requirements and to be isolated. The latter criterion is particularly important as the analysis targets the identification of events featuring a large multiplicity of isolated jets and leptons.

The signal selection process considers leptons with properties fulfilling

$$p_T > 20 \text{ GeV} \quad \text{and} \quad |\eta| < 2.5 \text{ (electrons) or } 2.4 \text{ (muons)} \ . \tag{1}$$

Jets are reconstructed using the anti-k_T algorithm [31] with a distance parameter $R = 0.4$, and the analysis is restricted to jets featuring

$$p_T > 40 \text{ GeV} \quad \text{and} \quad |\eta| < 2.4 \ . \tag{2}$$

In addition, all jets that are overlapping with a lepton are discarded, the overlap being defined by constraining the angular distance in the transverse plane ΔR so that it is smaller than 0.4. The angular distance is defined in a standard way, with

$$\Delta R \equiv \sqrt{(\eta_j - \eta_\ell)^2 + (\varphi_j - \varphi_\ell)^2} > 0.4 \ , \tag{3}$$

where η_j (η_ℓ) is the jet (lepton) pseudo-rapidity and φ_j (φ_ℓ) is the corresponding azimuthal angle.

At the same time, lepton isolation requirements [32] restrict the amount of hadronic activity around the leptons, this activity being evaluated by including the contributions of all (isolated and non-isolated) jets and by ignoring any p_T requirement on the jets. Lepton isolation is enforced by means of three variables: first the mini-isolation variable defined as the scalar sum of the transverse momenta of all charged hadrons, neutral hadrons and photons within a cone of radius depending on the lepton p_T; then the ratio of the lepton p_T to the one of the closest jet within a $\Delta R = 0.4$ distance; and finally the p_T^{rel} variable defined as the transverse momentum of the lepton relative to the residual momentum of the closest jet (within a $\Delta R = 0.4$ angular distance from the lepton), after having subtracted the lepton momentum.

Since the analysis requires typically many jets and b-tagged jets (as much as at least four in one of the analysis signal regions, for instance), controlling precisely the performance of the b-tagging algorithm is critical. The considered CMS analysis relies a deep neural network algorithm, named DeepCSV [33], with a medium working point. The corresponding b-tagging efficiency $\mathcal{E}_{b|b}$ approximately reads

$$\mathcal{E}_{b|b}(p_T) = \begin{cases} 0.13 + 0.028\ p_T - 5.07{\cdot}10^{-4}\ p_T^2 + 4.07{\cdot}10^{-6}\ p_T^3 - 1.21{\cdot}10^{-8}\ p_T^4 \\ \qquad \text{for } \ 25 \text{ GeV} < p_T < 115 \text{ GeV} \ , \\ 0.65 + 0.00143\ p_T - 1.03{\cdot}10^{-5}\ p_T^2 + 2.55{\cdot}10^{-8} p_T^3 - 2.78{\cdot}10^{-11} \\ \qquad p_T^4 + 1.11 \cdot 10^{-14} p_T^5 \quad \text{for } 115 \text{ GeV} \leqslant p_T < 950 \text{ GeV} \ , \\ 0.50 \quad \text{for } \ p_T \geqslant 950 \text{ GeV} \ , \end{cases} \tag{4}$$

and is associated with the mistagging rate of a charmed jet ($\mathcal{E}_{b|c}$) and a light jet ($\mathcal{E}_{j|b}$) as a b-jet given by

$$\mathcal{E}_{b|c}(p_T) = \begin{cases} 0.0571 + 0.00603\ p_T - 1.74{\cdot}10^{-4}\ p_T^2 + 2.15{\cdot}10^{-6}\ p_T^3 - 1.20{\cdot}10^{-8}\ p_T^4 \\ \quad +2.50{\cdot}10^{-11}\ p_T^5 \quad \text{for} \quad 25\ \text{GeV} < p_T < 155\ \text{GeV}\ , \\ 15.8 - 0.432\ p_T + 4.87{\cdot}10^{-3}\ p_T^2 - 2.88{\cdot}10^{-5}\ p_T^3 + 9.43{\cdot}10^{-8}\ p_T^4 \\ \quad -1.62{\cdot}10^{-10}\ p_T^5 + 1.14{\cdot}10^{-13}\ p_T^6 \quad \text{for} \quad 155\ \text{GeV} < p_T < 318\ \text{GeV}\ , \\ 0.119 - 0.000225\ p_T + 1.36{\cdot}10^{-6}\ p_T^2 - 1.96{\cdot}10^{-9}\ p_T^3 + 7.38{\cdot}10^{-13}\ p_T^4 \\ \quad +1.11{\cdot}10^{-16}\ p_T^5 \quad \text{for} \quad 318\ \text{GeV} \leqslant p_T < 950\ \text{GeV}\ , \\ 0.14 \quad \text{for} \quad p_T \geqslant 950\ \text{GeV}\ , \end{cases}$$

$$\mathcal{E}_{b|j}(p_T) = \begin{cases} 0.0194 - 0.000344\ p_T + 3.66{\cdot}10^{-6}\ p_T^2 - 1.43{\cdot}10^{-8}\ p_T^3 + 1.27{\cdot}10^{-11}\ p_T^4 \\ \quad +4.82{\cdot}10^{-14}\ p_T^5 - 8.56{\cdot}10^{-17}\ p_T^6 \quad \text{for} \quad 25\ \text{GeV} < p_T < 360\ \text{GeV}\ , \\ 1.26 - 0.0134\ p_T + 5.83{\cdot}10^{-5}\ p_T^2 - 1.30{\cdot}10^{-7}\ p_T^3 + 1.57{\cdot}10^{-10}\ p_T^4 \\ \quad -9.79{\cdot}10^{-14}\ p_T^5 + 2.48{\cdot}10^{-17}\ p_T^6 \quad \text{for} \quad 260\ \text{GeV} \leqslant p_T < 950\ \text{GeV}\ , \\ 0.035 \quad \text{for} \quad p_T \geqslant 950\ \text{GeV}\ . \end{cases} \tag{5}$$

We have accordingly designed a customised DELPHES 3 [34] card, which should be used for the simulation of the detector response associated with our implementation (see below). The above performance corresponds to an average tagging efficiency ranging 50% and 70%, for quite small associated false positive rates.

In the CMS-TOP-18-003 analysis, signal b-jet candidates are selecting by enforcing their transverse momentum to satisfy

$$p_T > 25\ \text{GeV}\ . \tag{6}$$

2.2. *Event selection*

Strong selection cuts are then applied to unravel the signal from the large background. One first requires event final states to exhibit the presence of at least two jets ($N_j \geq 2$) and two b-tagged jets ($N_b \geq 2$), and then constrains the sum of the transverse momenta of all reconstructed jets to satisfy

$$H_T = \sum_{i=1}^{N_j} > 300\ \text{GeV}\ . \tag{7}$$

As a sensible amount of missing transverse energy p_T^{miss} is expected to arise from the leptonic top-quark decays for the considered signal, we ask events to satisfy

$$p_T^{\text{miss}} > 50\ \text{GeV}\ . \tag{8}$$

Table 1. Preselection cuts as defined in the CMS-TOP-18-003 analysis [4]. We recall that the sum of the transverse momenta of all jets is given by H_T, as defined in Eq. (7).

Basic kinematic requirements				
	Electrons	Muons	Jets	b-tagged jets
p_T (GeV)	> 20	> 20	> 40	> 25
η (GeV)	> 2.5	> 2.4	> 2.4	> 2.4
Baseline selection				
Jets	$H_T > 300$ GeV, $p_T^{\rm miss} > 50$ GeV, at least two jets and two b-tagged jets			
Leptons	If same charge pair: $p_T(\ell_1) > 25$ GeV and $p_T(\ell_i) > 20$ GeV for $i \neq 1$			
Isolation	Jets and b-tagged jets $\Delta R > 0.4$ w.r.t the selected leptons			
Further vetoes				
Vetoed	Same sign electron pairs with pair mass below 12 GeV			
Vetoed	Third lepton with $p_T > 5(7)$ GeV for e (μ) forming an opposite-sign same-flavour pair with an invariant mass $m_{\rm OS} < 12$ GeV or $m_{\rm OS} \in [76, 106]$ GeV			

Table 2. Definition of the signal regions of the CMS-TOP-18-003 analysis, together with the expectation from SM $t\bar{t}t\bar{t}$ production as reported by the CMS collaboration (pre-fit results are shown) [4].

N_ℓ	N_b	N_j	Region	$t\bar{t}t\bar{t}$ (SM - CMS)
2	2	6	SR1	1.89 ± 1.14
2	2	7	SR2	1.04 ± 0.57
2	2	$\geq$8	SR3	0.67 ± 0.38
2	3	5	SR4	1.51 ± 0.85
2	3	6	SR5	1.61 ± 0.90
2	3	7	SR6	1.14 ± 0.66
2	3	$\geq$8	SR7	0.85 ± 0.47
2	≥ 4	$\geq$5	SR8	2.08 ± 1.23

N_ℓ	N_b	N_j	Region	$t\bar{t}t\bar{t}$ (SM - CMS)
≥ 3	2	5	SR9	0.66 ± 0.38
≥ 3	2	6	SR10	0.33 ± 0.21
≥ 3	2	$\geq$7	SR11	0.22 ± 0.13
≥ 3	≥ 3	4	SR12	0.56 ± 0.32
≥ 3	≥ 3	5	SR13	0.66 ± 0.38
≥ 3	≥ 3	$\geq$6	SR14	0.76 ± 0.45

As usual $p_T^{\rm miss}$ denotes the magnitude of the projection of the negative sum of the momenta of all reconstructed candidates in the event on the plane perpendicular to the beams.

One then restricts the kinematical properties of the leptons and enforce that the leading lepton has a transverse momentum $p_T(\ell_1) > 25$ GeV and that there exists a trailing lepton of the same electric charge with a $p_T(\ell_i) > 20$ GeV (with $i \neq 1$). In addition, events featuring more than two leptons are allowed, provided that no other same-sign lepton pair can be formed with the leading lepton.

Extra selections are imposed to reject the possibility that a lepton pair originates from a hadronic resonance or from a Z-boson decay. The invariant mass $m_{\ell\ell}$ of any electron pair and any opposite-sign muon pair that can be formed from the leptonic content of the event has to be larger than 12 GeV. Moreover, $m_{\ell\ell}$ has to lie outside the Z-boson mass window in the case of an opposite-sign same-flavour pair ($m_{\ell\ell} \notin [76, 106]$ GeV). Those preselection cuts are summarised in Table 1.

Once signal leptons, jets and b-tagged jets have been identified and selected, the CMS analysis then splits all surviving events into 14 distinct signal regions (SR), according to the number of leptons present in the event N_ℓ, as well as the number

of b-jets N_b and jets N_j. This selection is summarised signal region by signal region, in Table 2, along with the predicted number of SM $t\bar{t}t\bar{t}$ events that is expected for each SR. The selection cuts are very stringent and typically retain only around 2% of the cross section.

Very importantly, one should pay attention to how the numbers of SM four-top events populating each signal region are reported by the CMS collaboration. The final results are provided "post-fit", *i.e.* after the cross section related to the four-top SM signal has been fitted so that theory and measurement match. In order to recover proper predictions, one needs to rescale the results by the theoretical cross section $\sigma_{4t}^{\rm SM}$. The obtained numbers of events, referred to henceforth as "pre-fit", are the values to be compared with our MadAnalysis 5 predictions when validation is at stake.

3. Validation

3.1. *Event generation*

In order to validate our implementation, we generate SM four-top signal events at the next-to-leading-order (NLO) accuracy in the strong coupling, convoluting NLO matrix elements with the NLO set of NNPDF3.0 parton densities [35] that is provided through the LHAPDF 6 library [36]. In our simulations, we set the factorisation and renormalisation scales to the average transverse mass of the final-state particles, and the corresponding scale variation uncertainties are obtained by varying this choice by a factor of two up and down. Parton density uncertainties are extracted using replicas sets.

After including the top quark decay with the MadSpin package [37] (so that spin correlations are retained) and MadWidth [38], the hard-scattering fixed-order results are matched with parton showers as described by Pythia 8 [39] that further includes the simulation of the hadronisation effects. We finally model the response of the CMS detector with Delphes 3 [34], which internally relies on FastJet [40] for object reconstruction.

We have created our own Delphes 3 card for this analysis, in order to match accurately the lepton and jet reconstruction efficiencies as required by the CMS-TOP-18-003 analysis and the corresponding b-tagging performance [4] described in Section 2.1.

Our validation relies on 2,500,000 simulated SM events, generated according to the procedure described above. This leads to about 50,000 events passing all selection cuts. Accordingly, this allows us to neglect the statistical uncertainties with respect to the theoretical ones when validation histograms and cutflows are extracted.

3.2. *Comparison with the official results*

We validate our implementation of the CMS-TOP-18-003 analysis by comparing predictions obtained with our MadAnalysis 5 implementation and the SM four-

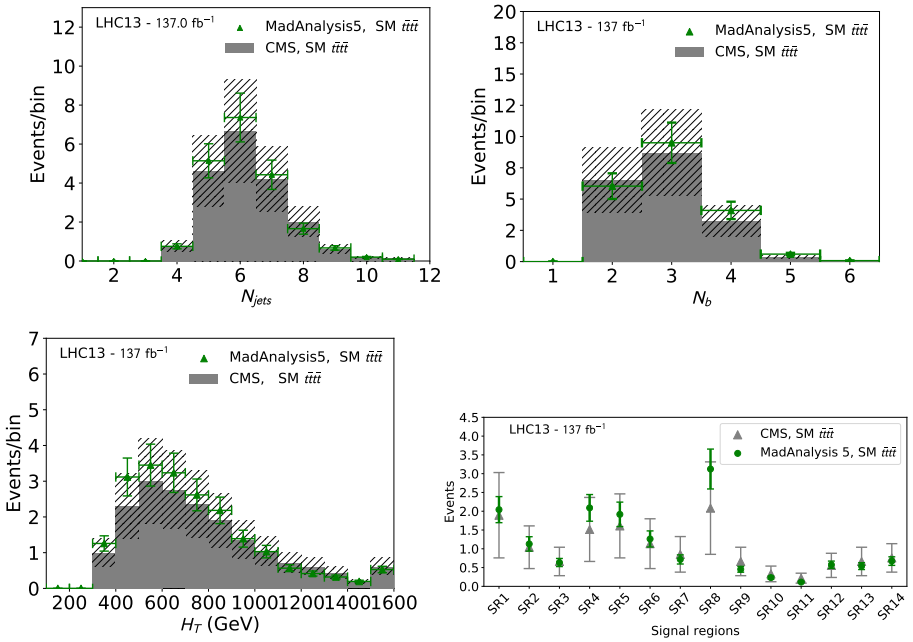

Fig. 1. Validation figures of our implementation, in the MadAnalysis 5 framework, of the CMS four-top analysis of Ref. [4]. We compare MadAnalysis 5 predictions (green) with the CMS official results (dark grey) for the jet multiplicity (upper-left panel), b-jet multiplicity (upper-right panel) and H_T (central-left panel) spectra, as well as for the event counts populating each signal region (lower right panel). The MadAnalysis 5 predictions include theoretical uncertainties (green error bars) whilst the CMS numbers include both systematical and statistical errors (black dashed bands and light grey error bars in the lower panel).

top events generated following the above strategy. We show in Fig. 1 the result of such a comparison for various differential distributions, and display histograms representing the jet multiplicity N_j (upper left), the b-jet multiplicity N_b (upper right) and the hadronic activity H_T (lower left). We find in all three cases a very good agreement, after accounting for the errors, between the MadAnalysis 5 predictions (green) and the CMS official results [4] (grey).

Moreover, we also present the event yields in the different signal regions (lower right) and compare again the MadAnalysis 5 numbers (green) to the CMS results (grey). A very good agreement is found, for all signal region.

We therefore consider our implementation as validated, so that it will be added to the MadAnalysis 5 Public Analysis Database (PAD) in a close future.

4. A practical example: top-philic scalars

As a simple illustrative example, we consider a simplified ($SU(2)$-violating) model in which a top-philic real scalar S of mass M_S interacts with the Standard Model

Table 3. Observed and limits on the considered new physics signal production rate, as obtained with MadAnalysis 5 and by using the implementation of the CMS-TOP-18-003 analysis [4]. We consider two scenarios for which $M_S = 600$ GeV (upper row) and $M_S = 1000$ GeV (lower row). We moreover also show the projected limits at the HL-LHC.

	SR1	SR2	SR3	SR4	SR5	SR6	SR7	SR8	SR9	SR10	SR11	SR12	SR13	SR14
$M_S = 600$ GeV														
$\sigma^{\rm lim}_{\rm obs}$ (fb)	86	70	124	55	29	97	49	**23**	169	363	979	87	95	80
$\sigma^{\rm lim}_{\rm HL-LHC}$ (fb)	26	29	34	19	**13**	16	19	12	58	65	351	26	23	21
$M_S = 1000$ GeV														
$\sigma^{\rm lim}_{\rm obs}$ (fb)	74	49	61	50	25	74	25	**17**	125	175	189	100	78	45
$\sigma^{\rm lim}_{\rm HL-LHC}$ (fb)	22	20	17	17	11	12	10	**9**	43	32	68	30	18	13

through the top-quark. The corresponding new physics Lagrangian reads

$$\mathcal{L}_{s0} \supset \frac{1}{2}\partial_\mu S \partial^\mu S - \frac{1}{2} M_S^2 S^2 + y_0 \bar{t} t \; S + h.c \; , \tag{9}$$

where y_0 denotes the new Yukawa coupling. The main production mechanism of the four-top signal induced by new physics, when $M_S > 2m_t$ and M_S is around or below the TeV-scale proceeds via associated production,

$$pp \to t\bar{t}S \to t\bar{t}t\bar{t} \; . \tag{10}$$

For lower scalar masses, the on-shell production of the scalar S dominates, implying that the cross section scales as y_0^2. On the contrary, for higher mass, the off-shell contribution dominates instead, so that the cross section scales as y_0^4.

We present in Table 3 limits on the new physics signal cross section that we derive with our MadAnalysis 5 implementation. We consider two scenarios in which $M_S = 600$ GeV and $M_S = 1000$ GeV respectively, and show results for each SR of the analysis. We observe that the strongest limits arise for the SR4, SR5 and SR8 region. The lack of sensitivity of the SR6 region is associated with an observed large upward fluctuation of events in CMS data. We moreover present projections for the HL-LHC as derived with the machinery introduced in Ref. [41].

Next, we scan over the singlet mass in the $[400, 1200]$ GeV range, and translate the limits on the cross section as a direct constraint on the S coupling to the top quark. We remind that $t\bar{t}S$ associated production typically dominates for such mass values. We present limits derived from the CMS analysis under consideration (blue), as well as projections for the HL-LHC (green) in Fig. 2. The regions above the blue and green thick line in the figure correspond to a 95% confidence level exclusion by the CMS-TOP-18-003 analysis when considering the run 2 and HL-LHC luminosity respectively. In order to derive these limits, we use standard build-in features from MadAnalysis 5 allowing for the calculation of the exclusion confidence level associated with a given signal. These are extensively documented in ref. [30]. The large error bars (corresponding to the shaded regions in the figure) are related to the significant theoretical uncertainties associated with our leading-order signal simulations. We refer to ref. [42] for a more refined analysis.

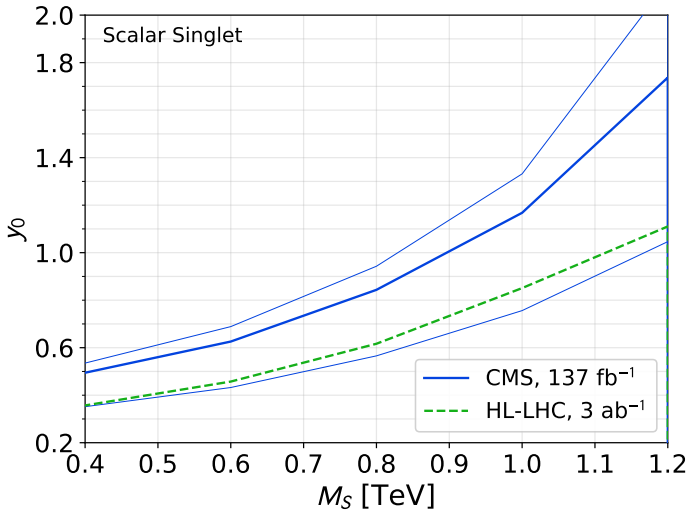

Fig. 2. Limit on y_0 as a function of masses derived from the above procedure in MadAnalysis 5 along with projections for the HL-LHC based on 3 ab^{-1} of data. The regions above the curves are excluded, and the shaded areas show the associated theoretical uncertainties for both limits.

At face value, the additional statistics provided by the HL-LHC imply a 50% improvements in the limits. However, the new physics signal is expected to strongly deviate from the SM background in various observables, such as the sum of the transverse momenta of all reconstructed jets H_T. One can therefore expect a significant improvement on these limits from a dedicated search strategy, as already mentioned in Ref. [22].

5. Conclusions

We have described in this work the implementation of the CMS-TOP-18-003 analysis in the MadAnalysis 5 framework. Such an analysis can be used to target new physics expected to show up in four-top events at LHC. We have validated our work by comparing predictions relying on the Monte Carlo simulations of SM four-top production. We have found an agreement with the CMS official results, well within their 1σ uncertainties. In particular, all the SR event counts agree with the CMS $t\bar{t}t\bar{t}$ projection within 30%, as do the differential distributions in H_T, $N_{\rm jets}$ and N_b. Consequently, the present work can be considered as validated and used without restriction to probe and test novel new physics models.

As an illustrative example of usage, we have reintepreted the CMS-TOP-18-003 analysis to extract bounds on a simplified top-philic scalar model, together with their projection at the HL-LHC.

The MadAnalysis 5 C++ code is available from the MA5 dataverse (https://doi.org/10.14428/DVN/OFAE1G) [43].

Acknowledgments

LD is supported by the INFN "Iniziativa Specifica" Theoretical Astroparticle Physics (TAsP-LNF).

References

1. R. Frederix, D. Pagani and M. Zaro, *JHEP* **02**, 031 (2018), arXiv:1711.02116 [hep-ph].
2. CMS Collaboration, A. M. Sirunyan *et al.*, *Eur. Phys. J. C* **78**, 140 (2018), arXiv:1710.10614 [hep-ex].
3. ATLAS Collaboration, M. Aaboud *et al.*, *JHEP* **12**, 039 (2018), arXiv:1807.11883 [hep-ex].
4. CMS Collaboration, A. M. Sirunyan *et al.*, *Eur. Phys. J. C* **80**, 75 (2020), arXiv:1908.06463 [hep-ex].
5. M. Battaglia and G. Servant, *Nuovo Cim. C* **033N2**, 203 (2010), arXiv:1005.4632 [hep-ex].
6. N. Greiner, K. Kong, J.-C. Park, S. C. Park and J.-C. Winter, *JHEP* **04**, 029 (2015), arXiv:1410.6099 [hep-ph].
7. E. Alvarez, D. A. Faroughy, J. F. Kamenik, R. Morales and A. Szynkman, *Nucl. Phys. B* **915**, 19 (2017), arXiv:1611.05032 [hep-ph].
8. J. H. Kim, K. Kong, S. J. Lee and G. Mohlabeng, *Phys. Rev. D* **94**, 035023 (2016), arXiv:1604.07421 [hep-ph].
9. P. J. Fox, I. Low and Y. Zhang, *JHEP* **03**, 074 (2018), arXiv:1801.03505 [hep-ph].
10. B. Lillie, J. Shu and T. M. Tait, *JHEP* **04**, 087 (2008), arXiv:0712.3057 [hep-ph].
11. A. Pomarol and J. Serra, *Phys. Rev. D* **78**, 074026 (2008), arXiv:0806.3247 [hep-ph].
12. N. Zhou, D. Whiteson and T. M. Tait, *Phys. Rev. D* **85**, 091501 (2012), arXiv:1203.5862 [hep-ph].
13. G. Cacciapaglia, H. Cai, A. Deandrea, T. Flacke, S. J. Lee and A. Parolini, *JHEP* **11**, 201 (2015), arXiv:1507.02283 [hep-ph].
14. G. Cacciapaglia, A. Deandrea, T. Flacke and A. Iyer, *JHEP* **05**, 027 (2020), arXiv:2002.01474 [hep-ph].
15. P. J. Fox, A. E. Nelson and N. Weiner, *JHEP* **08**, 035 (2002), arXiv:hep-ph/0206096.
16. T. Plehn and T. M. Tait, *J. Phys. G* **36**, 075001 (2009), arXiv:0810.3919 [hep-ph].
17. S. Choi, M. Drees, J. Kalinowski, J. Kim, E. Popenda and P. Zerwas, *Phys. Lett. B* **672**, 246 (2009), arXiv:0812.3586 [hep-ph].
18. D. Goncalves-Netto, D. Lopez-Val, K. Mawatari, T. Plehn and I. Wigmore, *Phys. Rev. D* **85**, 114024 (2012), arXiv:1203.6358 [hep-ph].
19. S. Calvet, B. Fuks, P. Gris and L. Valery, *JHEP* **04**, 043 (2013), arXiv:1212.3360 [hep-ph].
20. K. Benakli, M. Goodsell, F. Staub and W. Porod, *Phys. Rev. D* **90**, 045017 (2014), arXiv:1403.5122 [hep-ph].
21. W. Kotlarski, *JHEP* **02**, 027 (2017), arXiv:1608.00915 [hep-ph].
22. L. Darmé, B. Fuks and M. Goodsell, *Phys. Lett. B* **784**, 223 (2018), arXiv:1805.10835 [hep-ph].
23. M. Gerbush, T. J. Khoo, D. J. Phalen, A. Pierce and D. Tucker-Smith, *Phys. Rev. D* **77**, 095003 (2008), arXiv:0710.3133 [hep-ph].
24. A. Hayreter and G. Valencia, *Phys. Rev. D* **96**, 035004 (2017), arXiv:1703.04164 [hep-ph].

25. ATLAS Collaboration, M. Aaboud *et al.*, *Phys. Rev. D* **97**, 112001 (2018), arXiv:1712.02332 [hep-ex].
26. E. Alvarez, A. Juste and R. M. S. Seoane, *JHEP* **12**, 080 (2019), arXiv:1910.09581 [hep-ph].
27. E. Conte, B. Fuks and G. Serret, *Comput. Phys. Commun.* **184**, 222 (2013), arXiv:1206.1599 [hep-ph].
28. E. Conte, B. Dumont, B. Fuks and C. Wymant, *Eur. Phys. J. C* **74**, 3103 (2014), arXiv:1405.3982 [hep-ph].
29. B. Dumont, B. Fuks, S. Kraml, S. Bein, G. Chalons, E. Conte, S. Kulkarni, D. Sengupta and C. Wymant, *Eur. Phys. J. C* **75**, 56 (2015), arXiv:1407.3278 [hep-ph].
30. E. Conte and B. Fuks, *Int. J. Mod. Phys. A* **33**, 1830027 (2018), arXiv:1808.00480 [hep-ph].
31. M. Cacciari, G. P. Salam and G. Soyez, *JHEP* **04**, 063 (2008), arXiv:0802.1189 [hep-ph].
32. CMS Collaboration, V. Khachatryan *et al.*, *Eur. Phys. J. C* **76**, 439 (2016), arXiv:1605.03171 [hep-ex].
33. CMS Collaboration, A. Sirunyan *et al.*, *JINST* **13**, P05011 (2018), arXiv:1712.07158 [physics.ins-det].
34. DELPHES 3 Collaboration, J. de Favereau, C. Delaere, P. Demin, A. Giammanco, V. Lemaître, A. Mertens and M. Selvaggi, *JHEP* **02**, 057 (2014), arXiv:1307.6346 [hep-ex].
35. NNPDF Collaboration, R. D. Ball *et al.*, *JHEP* **04**, 040 (2015), arXiv:1410.8849 [hep-ph].
36. A. Buckley, J. Ferrando, S. Lloyd, K. Nordström, B. Page, M. Rüfenacht, M. Schönherr and G. Watt, *Eur. Phys. J. C* **75**, 132 (2015), arXiv:1412.7420 [hep-ph].
37. P. Artoisenet, R. Frederix, O. Mattelaer and R. Rietkerk, *JHEP* **03**, 015 (2013), arXiv:1212.3460 [hep-ph].
38. J. Alwall, C. Duhr, B. Fuks, O. Mattelaer, D. G. Öztürk and C.-H. Shen, *Comput. Phys. Commun.* **197**, 312 (2015), arXiv:1402.1178 [hep-ph].
39. T. Sjöstrand, S. Ask, J. R. Christiansen, R. Corke, N. Desai, P. Ilten, S. Mrenna, S. Prestel, C. O. Rasmussen and P. Z. Skands, *Comput. Phys. Commun.* **191**, 159 (2015), arXiv:1410.3012 [hep-ph].
40. M. Cacciari, G. P. Salam and G. Soyez, *Eur. Phys. J. C* **72**, 1896 (2012), arXiv:1111.6097 [hep-ph].
41. J. Y. Araz, M. Frank and B. Fuks, *Eur. Phys. J. C* **80**, 531 (2020), arXiv:1910.11418 [hep-ph].
42. L. Darmé, B. Fuks and F. Maltoni, *To appear* .
43. L. Darmé and B. Fuks, *https://doi.org/10.14428/DVN/OFAE1G* (2020).